Available online at www.sciencedirect.com

jmr&t Journal of Materials Research and Technology

journal homepage: www.elsevier.com/locate/jmrt

Original Article

Oxidation behavior of boron in 9CrMoCoB steel by CaF_2–CaO–Al_2O_3–SiO_2–B_2O_3 electroslag remelting (ESR) type slag

Sheng Chao Duan [a], *Min Joo Lee* [a], *Dong Soo Kim* [b], *Joo Hyun Park* [a,*]

[a] *Department of Materials Science and Chemical Engineering, Hanyang University, Ansan, 15588, South Korea*
[b] *Casting & Forging Business Unit, Nuclear Business Group, Doosan Heavy Industries & Construction, Changwon, 51711, South Korea*

ARTICLE INFO

Article history:
Received 17 September 2021
Accepted 6 January 2022
Available online 11 January 2022

Keywords:
9CrMoCoB steel
Electroslag remelting (ESR)
Ion-molecule coexistence theory (IMCT)
Oxidation
Boron
Silicon

ABSTRACT

The laboratory-scale experiments between the CaF_2–CaO–Al_2O_3–SiO_2–B_2O_3 slag and 9CrMoCoB steel were carried out in alumina and magnesia crucibles at 1823 K to investigate the oxidation behavior of boron (B) during the electroslag remelting (ESR) process. The activities of SiO_2 and B_2O_3 in the slag and the activities of Si and B in the molten steel were calculated by the ion and molecule coexistence theory (IMCT) and the Wagner formalism, respectively. The results showed that both SiO_2 and B_2O_3 have a significant influence on the equilibrium B content. The calculated content of B was in good agreement with the experimental value when the SiO_2+B_2O_3 content in the slag is more than 3.3 wt%. The temperature had little influence on the equilibrium B content when the SiO_2, B_2O_3 and CaO content were in the ranges of 3–5 wt%, 0–1 wt%, and 20–30 wt%, respectively. However, the Si is more prone to oxidation than is B as the temperature increases, indicating that more SiO_2 should be added in the slag to reduce the oxidation of Si. From the 80 tonnes industrial tests, the distribution of B and Si content along with the radial direction of the remelted ingot was almost uniform, which is in line with the calculated B content (approx. 30 ppm) under conditions of the Si content in the liquid steel and the (%B_2O_3)/(%SiO_2) ratio are 0.07% and 0.05, respectively, at 1973 K.

1. Introduction

About two-thirds of global electricity is produced from fossil fuel power plants with coal and natural gas as the primary fuels [1]. However, the use of these fuels is facing the dual pressures of high fuel consumption and environmental pollution [2]. To improve the net energy efficiency and reduce high CO_2 emissions associated with fossil fuel power plants, high efficiency of thermal power stations can be achieved by enhancing the steam temperatures and pressures [3]. These

* Corresponding author.
E-mail address: basicity@hanyang.ac.kr (J.H. Park).
https://doi.org/10.1016/j.jmrt.2022.01.033

Table 1 – Chemical reaction formulas of complex molecules that may be formed, their standard Gibbs free energy changes, and mass action concentration of structural units in 100 g of the CaF_2–CaO–Al_2O_3–SiO_2–B_2O_3 slags.

Reactions	ΔG_f^o (J/mol)	Mass action concentration (–)
$3(Ca^{2+}+O^{2-}) + (SiO_2) = (3CaO\cdot SiO_2)$	−118,826 - 6.694 T [50]	$N_{3CaO\cdot SiO_2} = K_{c1}N_{CaO}^3N_{SiO_2}$
$3(Ca^{2+}+O^{2-}) + 2(SiO_2) = (3CaO\cdot 2SiO_2)$	−236,814 + 9.623 T [50]	$N_{3CaO\cdot 2SiO_2} = K_{c2}N_{CaO}^3N_{SiO_2}^2$
$2(Ca^{2+}+O^{2-}) + (SiO_2) = (2CaO\cdot SiO_2)$	−102090 - 24.267T [51]	$N_{2CaO\cdot SiO_2} = K_{c3}N_{CaO}^2N_{SiO_2}$
$(Ca^{2+}+O^{2-}) + (SiO_2) = (CaO\cdot SiO_2)$	−21757 - 36.819 T [51]	$N_{CaO\cdot SiO_2} = K_{c4}N_{CaO}N_{SiO_2}$
$3(Ca^{2+}+O^{2-}) + (Al_2O_3) = (3CaO\cdot Al_2O_3)$	−21757 - 29.288 T [51]	$N_{3CaO\cdot Al_2O_3} = K_{c5}N_{CaO}^3N_{Al_2O_3}$
$12(Ca^{2+}+O^{2-}) + 7(Al_2O_3) = (12CaO\cdot 7Al_2O_3)$	617,977–612.119T [51]	$N_{12CaO\cdot 7Al_2O_3} = K_{c6}N_{CaO}^{12}N_{Al_2O_3}^7$
$(Ca^{2+}+O^{2-}) + (Al_2O_3) = (CaO\cdot Al_2O_3)$	59,413–59.413 T [51]	$N_{CaO\cdot Al_2O_3} = K_{c7}N_{CaO}N_{Al_2O_3}$
$(Ca^{2+}+O^{2-}) + 2(Al_2O_3) = (CaO\cdot 2Al_2O_3)$	−16736 - 25.522 T [51]	$N_{CaO\cdot 2Al_2O_3} = K_{c8}N_{CaO}N_{Al_2O_3}^2$
$(Ca^{2+}+O^{2-}) + 6(Al_2O_3) = (CaO\cdot 6Al_2O_3)$	−22594 - 31.798 T [50]	$N_{CaO\cdot 6Al_2O_3} = K_{c9}N_{CaO}N_{Al_2O_3}^6$
$3(Ca^{2+}+O^{2-}) + (B_2O_3) = (3CaO\cdot B_2O_3)$	−129790.8 - 54.6 T [52]	$N_{3CaO\cdot B_2O_3} = K_{c10}N_{CaO}^3N_{B_2O_3}$
$2(Ca^{2+}+O^{2-}) + (B_2O_3) = (2CaO\cdot B_2O_3)$	−108019.44 - 46.56 T [52]	$N_{2CaO\cdot B_2O_3} = K_{c11}N_{CaO}^2N_{B_2O_3}$
$(Ca^{2+}+O^{2-}) + (B_2O_3) = (CaO\cdot B_2O_3)$	−75362.4 - 20.77 T [52]	$N_{CaO\cdot B_2O_3} = K_{c12}N_{CaO}N_{B_2O_3}$
$(Ca^{2+}+O^{2-}) + 2(B_2O_3) = (CaO\cdot 2B_2O_3)$	−109694.16 - 0.67 T [52]	$N_{CaO\cdot 2B_2O_3} = K_{c13}N_{CaO}N_{B_2O_3}^2$
$9(Al_2O_3) + 2(B_2O_3) = (9Al_2O_3\cdot 2B_2O_3)$	−176749.5 + 58.27 T [52]	$N_{9Al_2O_3\cdot 2B_2O_3} = K_{c14}N_{Al_2O_3}^9N_{B_2O_3}^2$
$2(Al_2O_3) + (B_2O_3) = (2Al_2O_3\cdot B_2O_3)$	−91712 + 30.097 T [52]	$N_{2Al_2O_3\cdot B_2O_3} = K_{c15}N_{Al_2O_3}^2N_{B_2O_3}$
$3(Al_2O_3) + 2(SiO_2) = (3Al_2O_3\cdot 2SiO_2)$	−4354 - 10.467 T [52]	$N_{3Al_2O_3\cdot 2SiO_2} = K_{c16}N_{Al_2O_3}^3N_{SiO_2}^2$
$(Ca^{2+}+O^{2-}) + 2(SiO_2) + (B_2O_3) = (CaO\cdot 2SiO_2\cdot B_2O_3)$	−167116.3 + 38.46 T [52]	$N_{CaO\cdot 2SiO_2\cdot B_2O_3} = K_{c17}N_{CaO}N_{SiO_2}^2N_{B_2O_3}$
$2(Ca^{2+}+O^{2-}) + (Al_2O_3) + (SiO_2) = (2CaO\cdot Al_2O_3\cdot SiO_2)$	−116,315 - 38.911T [51]	$N_{2CaO\cdot Al_2O_3\cdot SiO_2} = K_{c18}N_{CaO}^2N_{Al_2O_3}N_{SiO_2}$
$(Ca^{2+}+O^{2-}) + (Al_2O_3) + 2(SiO_2) = (CaO\cdot Al_2O_3\cdot 2SiO_2)$	−4184 - 73.638 T [51]	$N_{CaO\cdot Al_2O_3\cdot 2SiO_2} = K_{c19}N_{CaO}N_{Al_2O_3}N_{SiO_2}^2$
$3(Ca^{2+}+O^{2-}) + 3(Al_2O_3) + (Ca^{2+}+2F^{2-}) = (3CaO\cdot 2Al_2O_3\cdot CaF_2)$	−44492 - 73.15 T [53]	$N_{3CaO\cdot 2Al_2O_3\cdot CaF_2} = K_{c20}N_{CaO}^3N_{Al_2O_3}^2N_{CaF_2}$
$11(Ca^{2+}+O^{2-}) + 7(Al_2O_3) + (Ca^{2+}+2F^{2-}) = (11CaO\cdot 7Al_2O_3\cdot CaF_2)$	−228,760 - 155.8 T [53]	$N_{11CaO\cdot 7Al_2O_3\cdot CaF_2} = K_{c21}N_{CaO}^{11}N_{Al_2O_3}^7N_{CaF_2}$
$3(Ca^{2+}+O^{2-}) + 2(SiO_2) + (Ca^{2+}+2F^{2-}) = (3CaO\cdot 2SiO_2\cdot CaF_2)$	−255,180 - 8.20T [54]	$N_{3CaO\cdot 2SiO_2\cdot CaF_2} = K_{c22}N_{CaO}^3N_{SiO_2}^2N_{CaF_2}$

enhancements, in turn, demand the use of more advanced materials with adequate creep strength, toughness, and heat resistance at elevated temperatures (up to 650 °C) [4]. The addition of small amounts of boron (B) into steels and alloys, such as 9CrMoCoB heat resistant steel, is considered a valid strategy to enhance these mechanical properties [5–7], as the B retards the coarsening of $M_{23}C_6$ particles and promotes the formation of fine grains in steels and alloys [8–12]. Therefore, it is indispensable to maintain the B content in the steels and alloys within a narrow target range.

The loss of B in steel is mainly a result of the alloying element reacting with soluble oxygen [O] and nitrogen [N] in the steel. Therefore, in the melting stage, B should be added after the steel melts have been deoxidized using oxidizable elements, *i.e.*, Ca, Al, and Si [6,13]. The addition of strong nitride-forming elements, such as Ti and Zr, can prevent B from combining with nitrogen in the steel [14]. A method of combining Al and Ti has been adopted by Melloy et al. [15], and Llewellyn and Cook [16] to ensure soluble B in liquid steels.

However, the unstable SiO_2 in electroslag remelting (ESR) type slag can also cause the oxidation loss of B in steel due to the following redox reaction that occurs at the slag/metal interface [17,18], which inevitably leads to the inhomogeneous distribution of the oxidative element from the bottom to top of the ingot during ESR of the B-containing steel [17].

$$4[B] + 3(SiO_2) = 2(B_2O_3) + 3[Si], \quad \Delta G_1^o = -97,920 - 91.2\,T\ (J/mol) \tag{1}$$

The activity of B_2O_3 in slag is one of the key parameters to control the homogeneous distribution of B in steel during the ESR process. Some attempts had been made to measure the Henrian activity coefficient of B_2O_3 in the CaO–B_2O_3 [19–21], MgO–B_2O_3 [22–24], SiO_2–B_2O_3 [25,26], Al_2O_3–B_2O_3 [27–29], MgO–B_2O_3–SiO_2 [30,31], CaO–B_2O_3–SiO_2 [32,33], CaO–B_2O_3–SiO_2–CaF_2 [34], and the CaO–MgO–B_2O_3–Al_2O_3–SiO_2 [35] slag systems. However, to the best of the authors' knowledge, the activity of B_2O_3 in ESR type slag has yet to be experimentally determined [36]. To overcome these issues, Kim et al. [17] developed an understanding of the relationship between [B]/[Si] ratio and $(B_2O_3)/(SiO_2)$ ratio based on industrial trials and optimized technological conditions that can be used for producing 120-tonne 9CrMoCoB ingot.

Recently, Peng et al. [37] calculated the activity of B_2O_3 in the 55CaF_2–20CaO–22Al_2O_3–3MgO-xSiO_2-yB_2O_3 (wt%) slag ($x \le 3$, $y \le 3$) at 1823 K using the agglomerated electron phase model. They found that the relationship between the activity coefficient of B_2O_3 ($\gamma_{B_2O_3}$) in the slag and temperature can be expressed as $\log \gamma_{B_2O_3} = -6,582/T$. There are many studies regarding control of Al and Ti loss during the ESR process [38–42], whereas a few fundamental studies have been conducted to systematically investigate the oxidation behavior of B by ESR type slag. To address this gap in knowledge, the present study systemically investigates the effect of each component in the CaF_2–CaO–Al_2O_3–SiO_2–B_2O_3 slag on the equilibrium content of B in 9CrMoCoB steel in the temperature range from 1823 to 1973 K. In addition, the calculated equilibrium B content was also confirmed by the results of slag/metal equilibrium experiments.

2. Thermodynamic consideration

According to Eq. (1), the relationship between the equilibrium content of B in 9CrMoCoB steel and three variables, *i.e.*, the composition of the CaF_2–CaO–Al_2O_3–SiO_2–B_2O_3 slag, the chemistry of consumable electrode and the temperature,

Table 2 – Chemical composition of steel (wt%).

C	Si	Mn	B	Al	Cr	O	N	Others[a]	Fe
0.12	0.07	0.09	0.0049	0.002	10.3	0.004	0.02	6.1	Bal.

[a] Mo + V + W + Co + Ni + Nb.

can be obtained by simple mathematical derivation, as shown in Eq. (2).

$$\log[\%B] = \frac{1}{4}\left\{\log\frac{a_{B_2O_3}^2}{a_{SiO_2}^3} + 3\log f_{Si} - 4\log f_B + 3\log[\%Si] - \left(\frac{5,114}{T} + 4.76\right)\right\} \quad (2)$$

where f_i are the activity coefficient of component i in the metal phase in reference to the 1 wt% standard state, a_i is the activity of component i in slag phase with reference to the pure solid Raoultian standard state. T is the absolute temperature (K).

It can be seen from Eq. (2) that calculating the relationships between equilibrium B content in 9CrMoCoB steel and each component in the CaF_2–CaO–Al_2O_3–SiO_2–B_2O_3 slag requires a couple of parameters. One such parameter is the activity of SiO_2 and B_2O_3 in the slag. The ion and molecule coexistence theory (IMCT) has been successfully applied to calculate the activities of components in CaF_2 containing slag used in the ESR process [43–46]. Therefore, the activity (mass action concentration, N_i) of each component in the slag can be determined using the reported activity model based on the IMCT in the present study [43,47]. The physical meaning of the N_i is mole fraction, *viz.*, the ratio of the equilibrium molar number n_i of structural unit i to the total molar number $\sum n_i$ in a closed system, which is consistent with the traditionally applied activity a_i in the slag, and the pure solid matter is chosen as the standard state [48,49]. Since the phase diagram of the CaF_2–CaO–Al_2O_3–SiO_2–B_2O_3 slag has not been reported so far, the complex molecules will be deduced by using subsystems of the five-component slag. According to the hypothesis of the IMCT [47], 22 kinds of complex molecules can be found in the slags at metallurgical temperatures. Chemical reaction formulas of the complex molecules, their standard Gibbs free energy changes, and mass action concentrations of structural units in the subsystems of the CaF_2–CaO–Al_2O_3–SiO_2–B_2O_3 slag are shown in Table 1. The modeling and solving processes used have been described elsewhere in detail [43].

Another important parameter for determining equilibrium B concentration is the activity coefficient $f_{i=B,\,Si}$ of B and Si which can be calculated using the Wagner equation [55], the chemical composition of the steel, and the interaction coefficients are listed in Tables 2 and 3, respectively. Final parameter to be considered is temperature. The melting point of the steel is about 1820 K, as calculated by FactSage™ 7.3 software. Fraser and Mitchell [56] reported that the temperature of the electrode-slag interface is close to the liquidus temperature of 9CrMoCoB steel, and its superheat does not exceed 20–30 K. The reaction temperature at slag bath-metal pool interface can be taken as 1973 K based on the results experimentally determined by previous researchers [57–60]. Therefore, the temperature range investigated during the ESR process was 1823–1973 K.

3. Experimental procedure

Reagent-grade powders of CaF_2 (Junsei chemical Co., Ltd.), Al_2O_3 (Sigma–Aldrich, Co.), SiO_2, and B_2O_3 (Samchun Pure Chemical Co., Ltd) were used as raw materials. $CaCO_3$ powders (Kanto Chemical Co., Inc.) were calcined at 1273 K for 10 h in a muffle furnace to produce CaO. The thoroughly mixed powders were melted at 1773 K in a graphite crucible under a high-purity Ar atmosphere to ensure complete melting and homogenization. Then, the liquid sample was quenched on the cooled copper plate and ground. The chemical composition of the slag is listed in Table 4.

Examination of the slag-metal reaction between CaF_2–CaO–Al_2O_3–SiO_2–B_2O_3 slag and heat-resistant steel was conducted in a super Kanthal electric resistance furnace with a $MoSi_2$ heating element (Fig. 1). The temperature of the furnace was controlled by a proportional-integral-derivative controller connected to a Pt-30wt.%Rh/Pt–6wt.%Rh reference thermocouple. The temperature was calibrated to 1823 K using another thermocouple prior to the experiment.

Table 4 – Composition of slag used in this study (wt%).

Variable	Slag Composition			
	CaF_2	CaO	Al_2O_3	SiO_2+B_2O_3
SiO_2 content				
S1	49.3	26.2	24.1	0.3
S2	48.8	26.0	23.9	1.3
S3	47.8	25.4	23.4	3.3
S4	46.8	24.9	22.9	5.3
B_2O_3 content				
B1	47.0	25.0	23.0	5.0
B2	46.9	24.9	22.9	5.2
B3	46.7	24.8	22.9	5.6
B4	46.5	24.7	22.8	6.0

Table 3 – Interaction coefficients were used in the present study [61].

e_i^j	B	N	O	Si	C	Al	Cr	Mn
B	0.038	770/T-0.337	−0.212	0.078	0.22	–	–	−0.00086
Si	0.2	0.005	−0.23	0.103	0.18	0.058	−0.0003	−0.0146

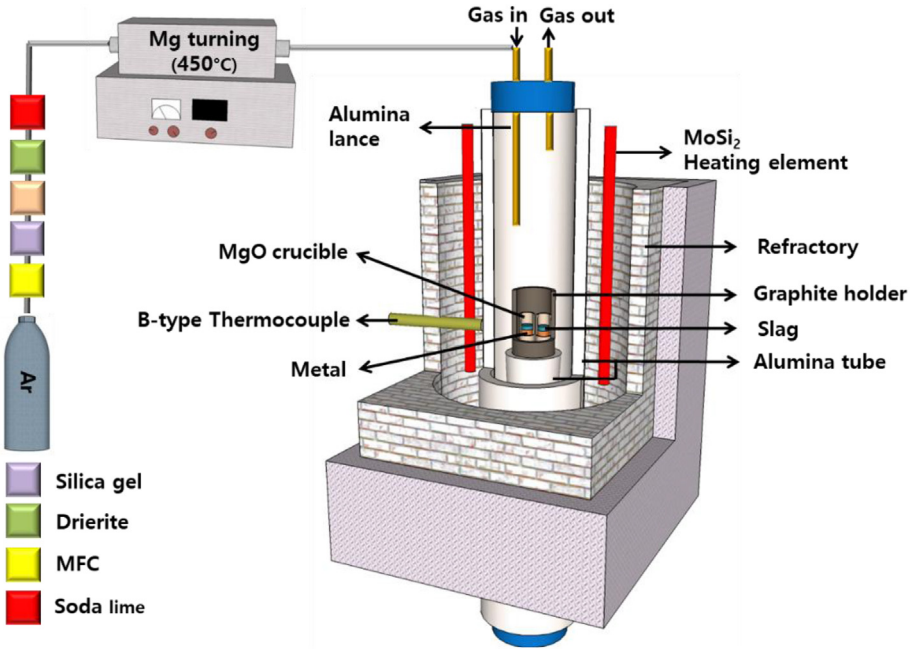

Fig. 1 – Schematic of the experimental equipment setup.

The master alloy (10 g) and slag mixture (5 g) were loaded into an Al_2O_3 crucible (15 mm outer diameter [OD], 12 mm inner diameter [ID], 50 mm height [HT]) and placed in a graphite holder (50 mm OD, 40 mm ID, 65 mm HT), which were linked with a molybdenum wire. When the furnace temperature reached the pre-set temperature of 1823 K, the graphite holder was then positioned in the constant zone of the resistance furnace. The reaction chamber was flushed by highly purified Ar gas at a constant rate to avoid oxidation of the steel. After 1 h of equilibration, the samples were quickly extracted from the furnace and quenched by dipping the crucible into brine.

After sampling, metal samples were polished using a grinder to remove the surface layer, which can affect the analysis results, then cut to a constant weight to reduce analytical error. Slag samples were ground and sized into 200 mesh sizes, and then prepared for chemical analysis. B, Si, and Al content in the metal samples and the composition of the slag were determined by inductively coupled plasma – atomic emission spectroscopy (ICP-AES, Spectro Arcos).

4. Results and discussion

4.1. *Relationship between equilibrium B content and slag composition at various temperatures*

As mentioned above, the activities of SiO_2 and B_2O_3 are the key parameters to control equilibrium B content in the steel. The calculated activity coefficient of B_2O_3 (B_2O_3<1.0 wt%) in the ESR type slag is about $\gamma_{B_2O_3} = 4.79 \times 10^{-4}$ at 1823 K in this study, which is close to the value $\gamma_{B_2O_3} = 2.45 \times 10^{-4}$ reported by Peng et al. [37] at the same temperature. Therefore, the relationships between the calculated B content for a given Si content (0.07%) and each component in the CaF_2–CaO–Al_2O_3–SiO_2–B_2O_3 slag in the temperature range from 1823 to 1973 K can be obtained from Eq. (2) based on the calculated activities of SiO_2 and B_2O_3 by the IMCT, and the results are shown in Fig. 2.

It can be seen from Fig. 2(a) that the equilibrium B content increases slightly with increasing CaF_2 content in the CaF_2–CaO–Al_2O_3–SiO_2–B_2O_3 slag at a fixed temperature. This result implies that the CaF_2 in the slag has little effect on the equilibrium B content. As shown in Fig. 2(b), the equilibrium B content decreases with increasing content of CaO when the CaO content in the slag is less than about 10%, while the equilibrium B content stays approximately the same value as the CaO content changes from 20% to 30%. The point of intersection between the calculated equilibrium B content and the iso-concentration line at 49 ppm (the initial B content in the steel as shown in Table 2) indicates that both B and Si in the liquid steel are not oxidized when the CaO content in the CaF_2–CaO–Al_2O_3–SiO_2–B_2O_3 slag is more than 20% at 1973 K. The effect of Al_2O_3 content on B content is not significant until 15% Al_2O_3, after which the equilibrium B content slightly increase with increasing content of Al_2O_3 as shown in Fig. 2(c). The equilibrium B content shows negative correlation with (%SiO_2)/(%B_2O_3) ratio in the slag, as shown in Fig. 2(d). The relationship between equilibrium B content and SiO_2 and B_2O_3 content is reliable when SiO_2+B_2O_3 content in the slag is

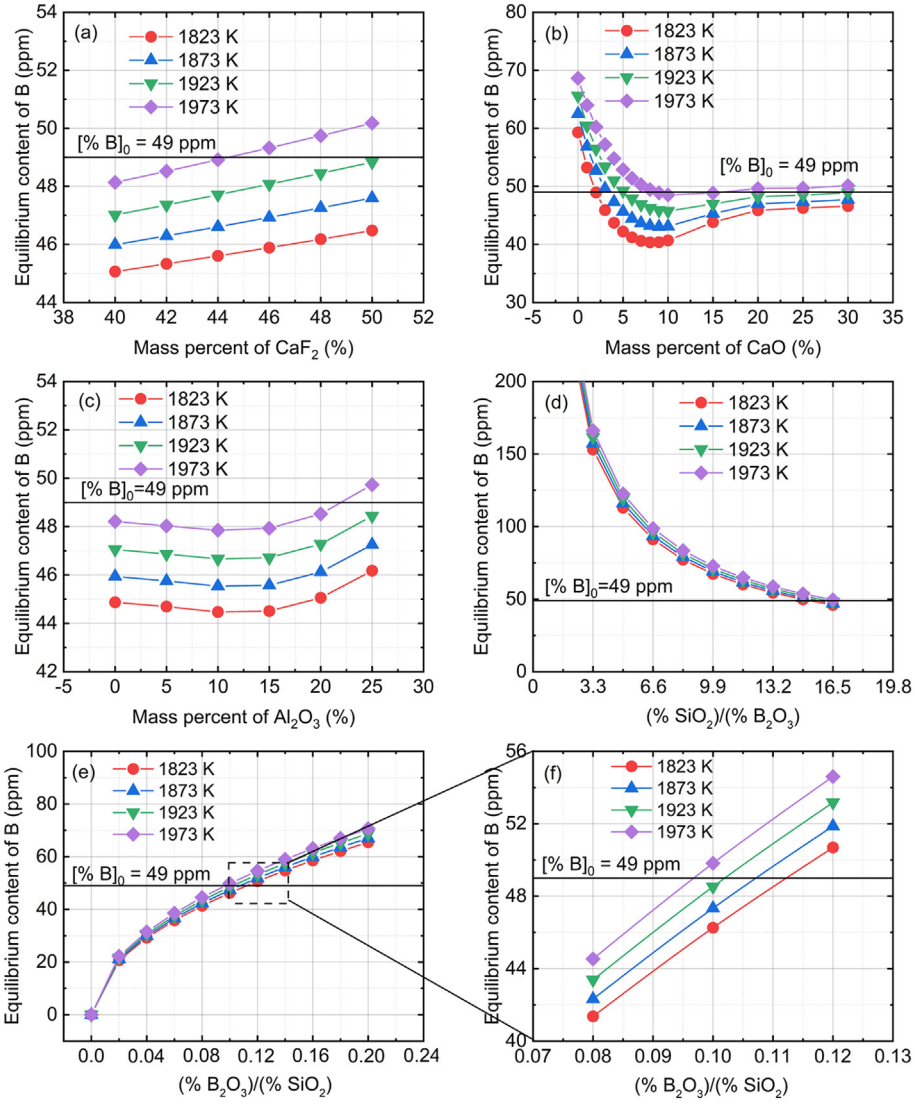

Fig. 2 – Relationship between equilibrium content of B for a given Si content (0.07%) and (a) CaF_2, (b) CaO, (c) Al_2O_3 content, (d) $(\%SiO_2)/(\%B_2O_3)$, and (e)–(f) $(\%B_2O_3)/(\%SiO_2)$ in the CaF_2–CaO–Al_2O_3–SiO_2–B_2O_3 slag in the temperature range from 1823 to 1973 K.

greater than about 3.3 wt%. In contrast, it can be seen from Fig. 2(e) that the equilibrium B content increases with an increase in $(\%B_2O_3)/(\%SiO_2)$ ratio up to 0.2. By comparing the results in Fig. 2, it can be understood that the relative order of importance of the components in the CaF_2–CaO–Al_2O_3–SiO_2–B_2O_3 slag for reducing the loss of B in molten 9CrMoCoB steel is: $B_2O_3 > SiO_2 > CaO > Al_2O_3 \approx CaF_2$.

Temperature is a key factor in controlling the equilibrium B content in 9CrMoCoB steel by the CaF_2–CaO–Al_2O_3–SiO_2–B_2O_3 slag during the ESR process. As can be observed in Fig. 2(b), the equilibrium B content increases with increasing temperature at a fixed slag composition when CaO content is less than 20%. These data indicate that the alloying element Si in the molten steel becomes more prone to oxidation than does B as the temperature rises, so extra SiO_2 should be added in the slag system. However, the oxidation loss of B in the liquid steel can also be mitigated by addition of 20%–30% CaO, hence high slag temperature can be adopted to remelt 9CrMoCoB steel. To keep the B content constant, such as at the iso-concentration line of [B] = 49 ppm, the amount of CaO should be increased with an increase in temperature from 1823 to 1973 K, as shown in Fig. 2(b) during the beginning stage of the ESR process. Similar results can be observed in Figs. 2(e) and (f). The CaF_2–CaO–Al_2O_3–SiO_2–B_2O_3 slag with $(\%B_2O_3)/(\%SiO_2) = 0.1$ can be recommended for remelting of 9CrMoCoB steel.

4.2. *Effect of refractory material on equilibrium B content in steel: alumina crucible*

As previously mentioned, both SiO_2 and B_2O_3 in the CaF_2–CaO–Al_2O_3–SiO_2–B_2O_3 slag have a significant effect on the equilibrium B content in liquid 9CrMoCoB steel. To test the

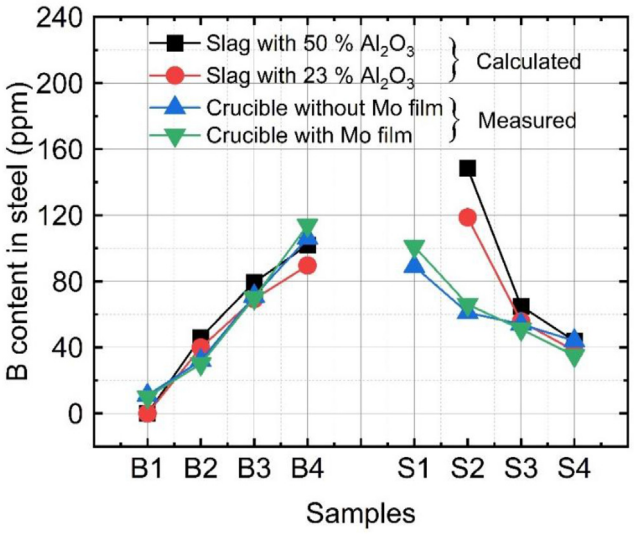

Fig. 3 – Comparisons between the calculated and measured B content in the liquid steel equilibrated with ESR type slags with various B_2O_3 (B1 to B4) and SiO_2 contents (S1 to S4) at 1823 K.

feasibility of the thermodynamic calculation method for the equilibrium B content in the liquid steel, the equilibrium B content was measured based on Eq. (1). Comparisons of the calculated and measured B content in the liquid steel equilibrated with ESR slags with various B_2O_3 (B1 to B4 in Table 4) and SiO_2 contents (S1 to S4 in Table 4) at 1823 K are shown in Fig. 3. The measured final slag composition of the slag-metal equilibrium experiments after 60 min is listed in Table 5. It can be observed from Fig. 3 that the calculated values of the equilibrium B content are in good agreement with the measured B content in the liquid steel equilibrated with B1 to B4, S3, and S4 slags at 1823 K. Whereas the calculated equilibrium B content is higher than the experimental values when the molten steel equilibrated with S1 and S2 slags. The reason for this deviation will be discussed later.

It is noted from Table 5 that the Al_2O_3 content in the slag after the slag-metal equilibrium experiment is nearly double that in the initial slag, as listed in Table 4, suggesting that dissolution of the Al_2O_3 crucible occurs upon contact with slag melts. Several researchers [62–66] have investigated the dissolution behavior of Al_2O_3 refractory in fluoride-containing slag melts. They found that the dissolution rate of Al_2O_3 increased with increasing temperature and CaF_2 content in slag due to the increase of mass transfer coefficient of Al_2O_3 and the reduced viscosity of the slag [67,68].

The predicted saturation concentration of Al_2O_3 in the CaF_2–CaO–Al_2O_3–SiO_2–B_2O_3 slag at 1823 K is about 60 wt% as determined by FactSage™ 7.3 software. The measured results are lower than the predicted values from the FactSage calculation, as displayed in Table 5. This discrepancy is likely due to the formation of intermediate compounds, such as $CaO{\cdot}6Al_2O_3$ and $CaO{\cdot}2Al_2O_3$, that occur at the interface between the Al_2O_3 crucible and the slag [65–70]; these intermediate compounds could suppress the direct dissolution of Al_2O_3 from the crucible to the slag [71,72].

To try to prevent the direct reaction between slag and refractory crucible, several authors have adopted the method of

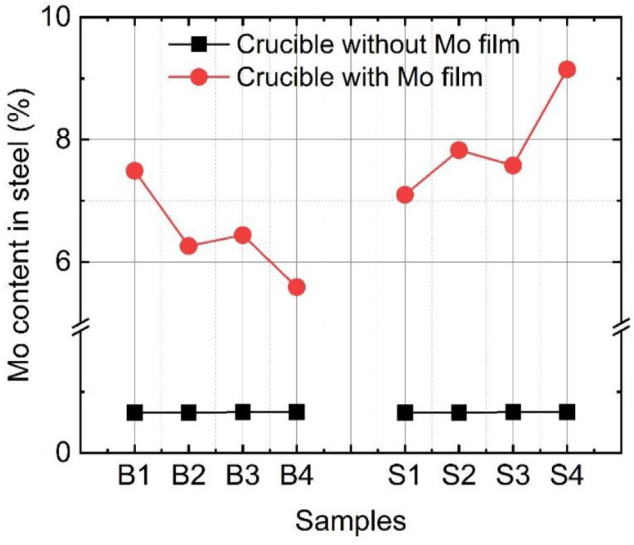

Fig. 4 – Change of Mo content in the liquid steel that was melted in an alumina crucible with and without a Mo foil lining at 1823 K.

Table 5 – Slag composition after slag-metal equilibrium experiments (wt%).

Slag No.	Al_2O_3 crucible without Mo foil			Al_2O_3 crucible with Mo foil			Slag No.	MgO crucible without Mo foil			
	Al_2O_3	SiO_2	B_2O_3	Al_2O_3	SiO_2	B_2O_3		SiO_2	Al_2O_3	B_2O_3	MgO
AS1	47.3	0.1	0.2	40.2	0.6	0.2	MS1	4.1	18.8	0.5	18.0
AS2	49.7	0.8	0.2	47.3	0.5	0.1	MS2	5.8	18.6	0.9	17.9
AS3	51.1	1.9	0.2	48.7	1.7	0.1					
AS4	50.3	3.1	0.2	42.9	2.8	0.1					
AB1	50.0	2.9	<0.1	33.6	2.7	<0.1					
AB2	52.1	3.0	0.1	43.1	2.9	0.1					
AB3	49.2	3.1	0.4	48.8	2.4	0.2	MB3	6.3	19.3	0.6	17.9
AB4	50.4	3.2	0.6	29.3	2.5	0.4	MB4	3.0	20.3	0.4	16.7

Note: "A" and "M" in slag sample ID means that the experiments are conducted using an Al_2O_3 or a MgO crucible, respectively.

lining the crucible with a molybdenum foil [37,43,46] to design the slag composition for simulating the oxidation of reactive elements in steels and alloys during the ESR process. Therefore, an alumina crucible lined with a 0.2-mm-thick molybdenum foil was used in the present study to investigate the oxidation behavior of B in the liquid steel by the CaF_2–CaO–Al_2O_3–SiO_2–B_2O_3 slag at 1823 K. The final slag composition after the slag-metal equilibrium reaction using the alumina crucible lined with Mo foil is detailed in Table 5. It can be seen from Table 5 that the slags contain an average of about 42 wt% Al_2O_3 because the part of the Mo foil in contact with the slag and metal corrodes at high temperature, even though the Mo foil is placed on the inner wall of the alumina crucible.

In addition, it is evident from Fig. 4 that the Mo content increases from 0.7% in the master alloy to 6%–8% in the steel samples after the slag-metal equilibrium experiments using an alumina crucible lined with Mo foil at 1823 K. It is interesting to note that the determined equilibrium B contents using crucibles with and without the Mo foil are consistent. These results imply that a change in the Mo content in the liquid steel has little effect on the equilibrium B content.

The relationship between Mo content and the calculated activities of B and Si in the liquid steel by FactSage™ 7.3 software at 1823 K is illustrated in Fig. 5. These data suggest that both the activities of B and Si remain basically unchanged with increasing Mo content from 0.7% to 8% in the liquid steel. As a result, the measured equilibrium B content maintains stable whether or not a Mo foil is used in the present study. From the results of these experiments, it is clear that the method of lining a crucible with a Mo foil is not effective in inhibiting the dissolution of an alumina crucible. However, the increased Al_2O_3 content only results in a slight increase of the equilibrium content of B in the liquid steel, as shown in Fig. 3. This phenomenon has been proven by the relationship between the calculated equilibrium B content and the Al_2O_3 content in the slag in the temperature range from 1823 to 1973 K, as shown in Fig. 2(c). These results demonstrate that the relationship between the calculated equilibrium content of B and the content of each component in the CaF_2–CaO–Al_2O_3–SiO_2–B_2O_3 slag at the temperature range from 1823 to 1973 K can be applied to design a slag composition that controls the oxidation loss of B during the ESR process.

4.3. *Effect of refractory material on equilibrium B content in steel: magnesia crucible*

Additional experiments were carried out using a magnesia crucible without Mo film to investigate the changes to the Si, Al, and B contents in the molten steel during the reaction between the molten steel and S1, S2, B3, and B4 slags at 1823 K. These experiments aim to elucidate why the calculated equilibrium B content is higher than those measured for low SiO_2 content, such as S1 and S2 slags, a phenomenon that can be observed in Fig. 3. The experimental procedure is described

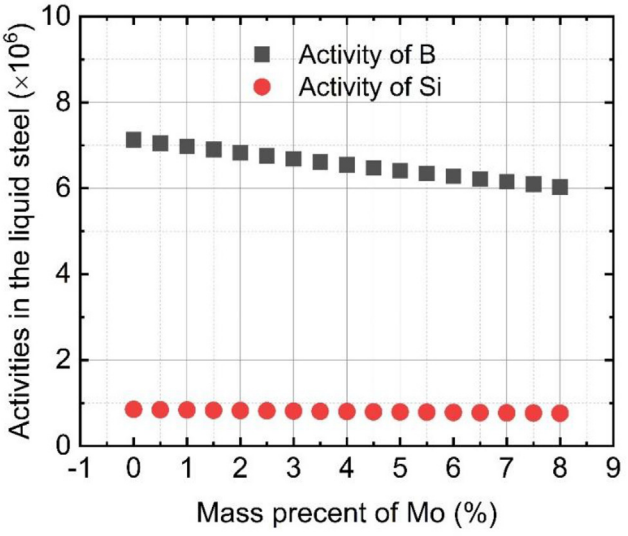

Fig. 5 – Relationship between Mo content and the activity of B and Si in the liquid steel at 1823 K, as calculated by FactSage™ 7.3 software. The activities of B and Si refer to the pure solid matter as standard state.

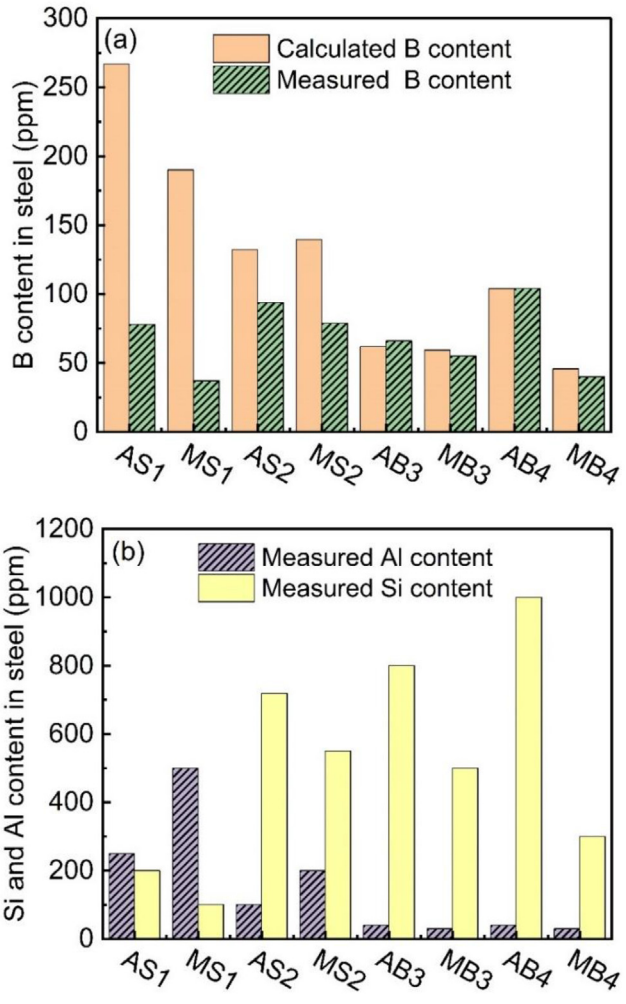

Fig. 6 – Changes to (a) B content, and (b) Si and Al contents in the molten steel during the reaction between the molten steel and slags S1, S2, B3, and B4 reacted at 1823 K. Note: "A" and "M" in the sample ID indicates that the experiments are conducted using Al_2O_3 or MgO crucibles, respectively.

in detail in Section 3. After a certain reaction period (60 min), both slag and metal samples were quickly taken from the furnace and quenched in brine. The experimental results are shown in Fig. 6.

Comparing Fig. 3 and Fig. 6(a) show similar trends in that the calculated B content is higher than the measured B content in the liquid steel equilibrated with Sl and S2 slags, whereas the calculated B content is in good agreement with the measured values when the liquid steel reacts with B3 and B4 slags in an alumina or a magnesia crucible. This deviation can be attributed to the fact that only the equilibrium reaction given in Eq. (1) is considered when calculating equilibrium B content based on the equilibrium Si content in the molten steel for slag systems containing low SiO_2 content, S1 (SiO_2+B_2O_3 = 0.3%), and S2 (SiO_2+B_2O_3 = 1.3%). Besides Eq. (1), the following reaction also simultaneously occurs:

$$4[Al] + 3(SiO_2) = 2(Al_2O_3) + 3[Si], \quad \Delta G_3^o = -720,680 + 133\,T\ (J/mol) \tag{3}$$

Comparison between the standard Gibbs free energy changes of Eqs. (1) and (3) is illustrated in Fig. 7(a). It can be seen that the standard Gibbs free energy change of Eq. (3) ($1/3\Delta G_3^o$ for 1 mol SiO_2) is lower than that of Eq. (1) ($1/3\Delta G_1^o$ for 1 mol SiO_2), indicating that the Si content in steel is mainly controlled by Eq. (3). The equilibrium Si contents in the molten steel calculated by Eqs. (1) and (3) are shown in Fig. 7(b), from which it can be obtained that the equilibrium Si content calculated by (SiO_2)-[Al] equilibrium is higher compared with that calculated by (SiO_2)-[B] equilibrium when the liquid steel reacts with low SiO_2 (S1, S2) slags.

According to classical metallurgical thermochemistry, both Eqs. (1) and (3) should be considered when calculating the equilibrium Si and B contents. This is why the calculated B contents are higher than the measured values for low SiO_2 content S1 and S2 slags in Fig. 6(a). However, with the increase of SiO_2 content in slag, such as in S2 to S4 and B1 to B4 slags, the determined values of Si content from (SiO_2)-[Al] and (SiO_2)-[B] equilibria are in good agreement, and the equilibrium B content in the liquid steel can be accurately calculated only using Eq. (1), even though the equilibrium Si content is predominantly controlled by Eq. (3). Therefore, the thermodynamic analysis results using Eq. (1) can be used to design slag composition for electroslag remelting of 9CrMoCoB steel with ($\%SiO_2$)/($\%B_2O_3$) ratio more than 10, as can be observed in Fig. 2.

It is interesting that the calculated Si contents (Fig. 7(b)) are in good agreement with the measured values (Fig. 6(b)), and that the measured Si content in the liquid steel equilibrated with MS1, MS2, MB3, and MB4 slags are lower than those in liquid steel equilibrated with AS1, AS2, AB3, and AB4 slags at 1823 K. It can be also seen from Table 5 that the MgO content

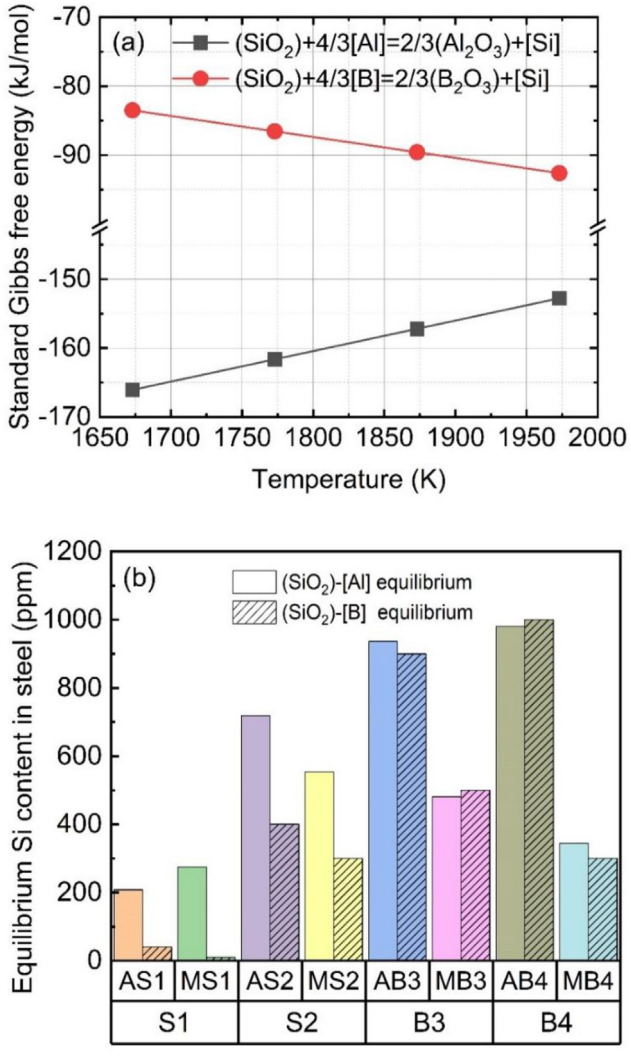

Fig. 7 – (a) Change of standard Gibbs free energies of Eqs. (1) and (3) for 1 mole SiO_2, and (b) calculated Si content in the steel equilibrated with S1, S2, B3, and B4 slags at 1823 K. Note: "A" and "M" in sample ID indicates that the experiments are conducted using an alumina or a magnesia crucible, respectively.

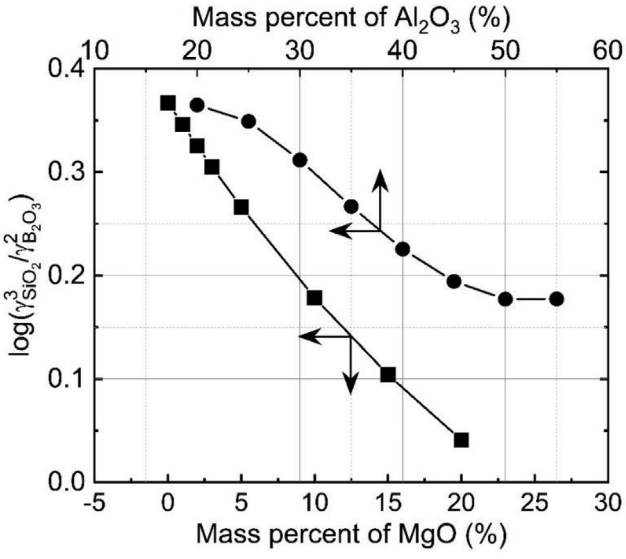

Fig. 8 – Relationship between Al_2O_3 and MgO content in the CaF_2–CaO–Al_2O_3–SiO_2–B_2O_3 slag and $\log\left(\gamma^3_{SiO_2}/\gamma^2_{B_2O_3}\right)$ at 1823 K.

increases from 0 to about 18 wt% when the slag-metal reactions between the liquid steel and S1, S2, B3, and B4 slags are conducted in a magnesia crucible, which is almost consistent with the 15 wt% value calculated by FactSage™ 7.3 software at 1823 K.

The dependence of the $\log\left(\gamma^3_{SiO_2}/\gamma^2_{B_2O_3}\right)$ of the Al_2O_3 and MgO content in the CaF_2–CaO–Al_2O_3–SiO_2–B_2O_3 slag at 1823 K is shown in Fig. 8. It is obvious that $\log\left(\gamma^3_{SiO_2}/\gamma^2_{B_2O_3}\right)$ sharply decreases with increasing Al_2O_3 and MgO content in the slag, indicating that the value of $\log([\%Si]^3/[\%B]^4)$ will also decreases. The change in MgO content in the CaF_2–CaO–Al_2O_3–SiO_2–B_2O_3 slag makes the values of $\log\left(\gamma^3_{SiO_2}/\gamma^2_{B_2O_3}\right)$ even lower, giving rise to the lower measured Si and B contents in the liquid steel equilibrated with MS1, MS2, MB3, and MB4 slags than those in the liquid steel equilibrated with AS1, AS2, AB3, and AB4 slags.

4.4. *Effect of Si content on equilibrium B content in liquid steel at 1873 K*

The relationship between the calculated B content and slag composition for different Si contents at 1873 K is shown in Fig. 9. In comparison to Fig. 2(d) and Fig. 2(e), Fig. 9 exhibits similar trends, but the Si content has more of an effect on the equilibrium content of B in the liquid steel than does temperature. Similarly, the influence of Si content in electrode on the B content in remelted ingot has been investigated by Kim et al. [17] in a study of industrial-scale electroslag remelting of 9CrMoCoB steel using the CaF_2–CaO–Al_2O_3–SiO_2–B_2O_3 slag. They observed that the equilibrium B content increased with an increase in B_2O_3 content in the slag and Si content in the electrode (from about 0.1 to 0.3 wt%). These results demonstrate that adjustment of Si content in the electrode is a more effective method for controlling the oxidation loss of B during the ESR process.

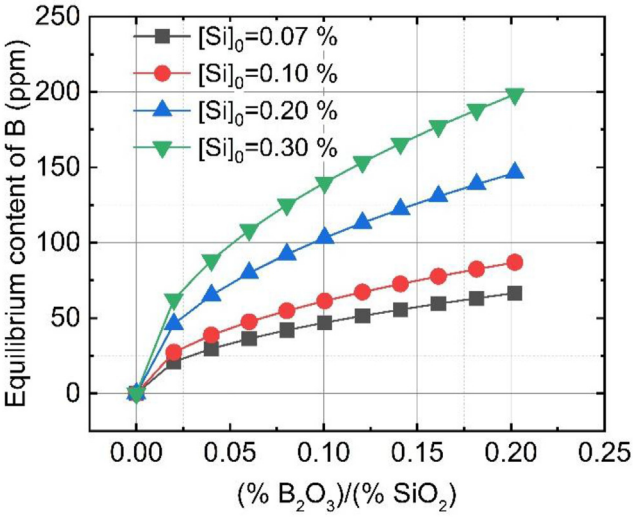

Fig. 9 – Relationship between equilibrium content of B in the liquid steel and ratio of mass percent of SiO_2 to B_2O_3 in the slag for various Si content in electrode at 1873 K.

Table 6 – Remelting parameters of 80 tonnes ESR operation.

Electrode	Size/weight	1600 mm/85 tonne
ESR conditions	Slag system	CaF_2–CaO–Al_2O_3–SiO_2–B_2O_3
	Starting method	Cold start
	Voltage swing	8 ~ 10 V
	Electrode surface	Shot blast
	Atmosphere	Ar gas

4.5. *Industrial trials*

To further testify the feasibility of the relationship between the slag composition and equilibrium B content in 9CrMoCoB steel at various temperatures as shown in Fig. 2, the 9CrMoCoB steel was employed as the consumable electrode with a diameter of 1600 mm and remelted at an industrial ESR furnace using the optimized slag composition. The relative parameters of 80 tonnes ESR operation are listed in Table 6. The metal samples were taken from the position 520 mm below the top part of the remelted ingot along with radial direction (diameter 2150 mm) for the analysis of the chemical

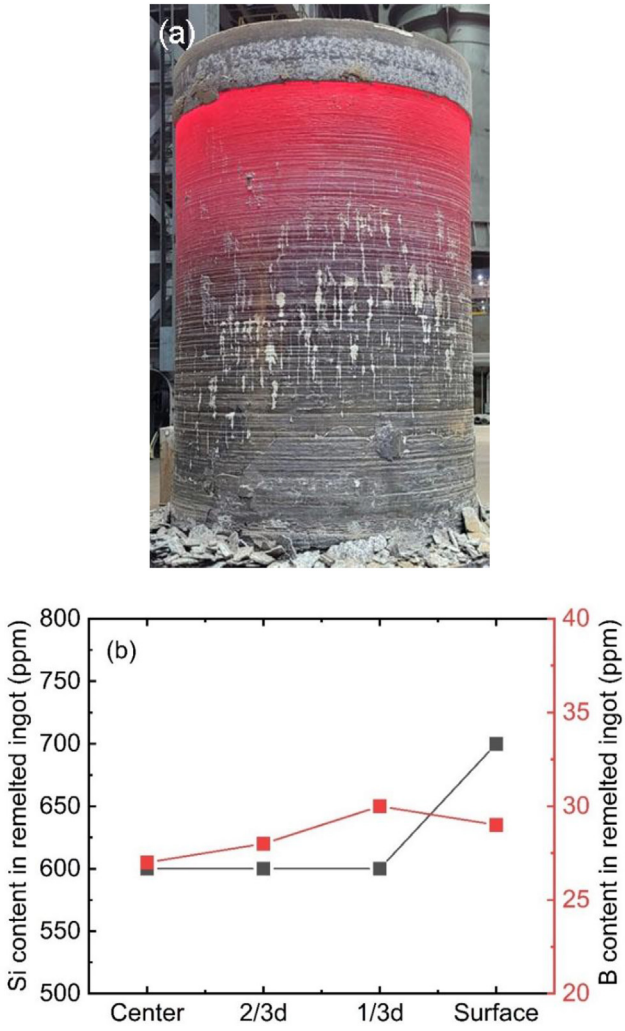

Fig. 10 – Picture of remelted ESR ingot (a) and Si and B content along with the radial direction of the remelted ingot (b).

composition since the reaction given in Eq. (1) can reach the equilibrium during the ESR process. The sampling locations along the radial direction are located at the center, 1/3 radius, 2/3 radius, and surface of the remelted ingot. The image of remelted ingot and the composition of the remelted ingot (Si and B contents) are shown in Fig. 10. It can be seen that the distribution of B and Si content along with the radial direction of the remelted ingot is almost uniform, which is in line with the calculated equilibrium B content (approx. 30 ppm) as shown in Fig. 2 under conditions of the Si content in the liquid steel and the ratio (% B_2O_3)/(% SiO_2) are 0.07% and 0.05, respectively, at 1973 K.

In summary, the ion and molecule coexistence theory (IMCT) can be reliably used to calculate the activity of B_2O_3 in the liquid CaF_2–CaO–Al_2O_3–SiO_2–B_2O_3 slag, and the thermodynamic analysis between the slag composition and equilibrium B content at the temperature range from 1823 to 1973 K can be applied to guide the slag design for control of the homogenous distribution of B and Si in 9CrMoCoB steel during the ESR process.

5. Conclusions

In the present study, the oxidation behavior of B in 9CrMoCoB steel by the CaF_2–CaO–Al_2O_3–SiO_2–B_2O_3 ESR type slag was theoretically and experimentally investigated, and the following main conclusions were obtained:

1) The equilibrium Si content in the steel is simultaneously controlled by reactions $4[B] + 3(SiO_2) = 2(B_2O_3) + 3[Si]$ and $4[Al] + 3(SiO_2) = 2(Al_2O_3) + 3[Si]$, and it was confirmed that the latter is thermodynamically dominant. The equilibrium B content can be accurately calculated based on the reaction $4[B] + 3(SiO_2) = 2(B_2O_3) + 3[Si]$ when the SiO_2+ B_2O_3 content in the slag is more than 3.3 wt%, as the Si contents controlled by (SiO_2)-[Al] and (SiO_2)-[B] equilibria are almost consistent with each other.
2) The relationships between each component in the CaF_2–CaO–Al_2O_3–SiO_2–B_2O_3 ESR type slag and the equilibrium B content in liquid 9CrMoCoB steel for a given Si content indicate that the order of importance of the slag components for reducing the loss of B in molten 9CrMoCoB steel is $B_2O_3 > SiO_2 > CaO > Al_2O_3 \cong CaF_2$.
3) Temperature is one of the key parameters that control the oxidation behavior of B in the liquid steel during the ESR process. The effect of temperature on the oxidation behavior of B in the liquid steel is different when the content of different components in the CaF_2–CaO–Al_2O_3–SiO_2–B_2O_3 ESR type slag change. The oxidation of Si is more prone to occur compared to that of Al when the temperature rises and the CaO content is less than 10%, whereas the temperature has little influence on the oxidation of Si and B when the CaO, B_2O_3, and SiO_2 contents are in the ranges of 20%–30%, 0%–1.0%, and 3%–5%, respectively.
4) The ratio [%Si]/[%B] in the steel melted in a magnesia crucible was lower than that melted in an alumina crucible due to the MgO in the slag makes the value of $\log\left(\gamma^3_{SiO_2}/\gamma^2_{B_2O_3}\right)$ even lower at 1823 K.
5) From the 80 tonnes industrial tests, the distribution of B and Si content along with the radial direction of the remelted ingot was almost uniform, which is in line with the calculated B content (approx. 30 ppm) under conditions of the Si content in the liquid steel and the (%B_2O_3)/(%SiO_2) ratio are 0.07% and 0.05, respectively, at 1973 K.

Declaration of Competing Interest

The authors declare that they have no known competing financial interests or personal relationships that could have appeared to influence the work reported in this research.

Acknowledgments

This work was supported by the research fund of Hanyang University, Korea (HY-2021).

REFERENCES

[1] Ang BW, Su B. Carbon emission intensity in electricity production: a global analysis. Energy Pol 2016;94:56–63. https://doi.org/10.1016/j.enpol.2016.03.038.
[2] Leonard MD, Michaelides EE, Michaelides DN. Energy storage needs for the substitution of fossil fuel power plants with renewables. Renew Energy 2020;145:951–62. https://doi.org/10.1016/j.renene.2019.06.066.
[3] Di Gianfrancesco A. Materials for ultra-supercritical and advanced ultra-supercritical power plants. United Kingdom: Woodhead Publishing; 2017. p. 1–49 [Chapter 1], The fossil fuel power plants technology.
[4] Hättestrand M, Andrén HO. Boron distribution in 9–12 % chromium steels. Mater Sci Eng, A 1999;270(Issue1):33–7. https://doi.org/10.1016/S0921-5093(99)00232-4.
[5] Yang K, Liang Y, Yan W, Shan Y. Preferential distribution of boron and its effect on microstructure and mechanical properties of (9~12) % Cr martensitic heat resistant steels. Acta Metall Sin 2020;56(Issue1):53–65. https://doi.org/10.11900/0412.1961.2019.00146.
[6] Sharma M, Ortlepp I, Bleck W. Boron in heat-treatable steels: a review. Steel Res Int 2019;90(Issue11):1900133. https://doi.org/10.1002/srin.201900133.
[7] Francis JA, Mazur W, Bhadeshia HKDH. Review Type IV cracking in ferritic power plant steels. Mater Sci Technol 2013;22(Issue12):1387–95. https://doi.org/10.1179/174328406x148778.
[8] Hasebe M, Nishizawa T. Thermodynamic analysis of the ternary Fe-C-B system. J Jpn Inst Met 1974;38(Issue1):46–54. https://doi.org/10.2320/jinstmet1952.38.1_46.
[9] Takahashi N, Fujita T, Yamada T. Effect of boron on long period creep rupture strength of 12 %Cr heat resisting steel.

Tetsu-To-Hagane 1975;61(Issue9):2263–73. https://doi.org/10.2355/tetsutohagane1955.61.9_2263.
[10] Lundin L, Andrén HO. Atom-probe investigation of a creep resistant 12 % chromium steel. Surf Sci 1992;266(Issue1):397–401. https://doi.org/10.1016/0039-6028(92)91052-D.
[11] Azuma T, Miki K, Tanaka Y, Ishiguro T. Effect of B on microstructural change during creep deformation in high Cr ferritic heat resistant steel. Tetsu-To-Hagane 2002;88(Issue10):678–85. https://doi.org/10.2355/tetsutohagane1955.88.10_678.
[12] Azuma T, Miki K, Tanaka Y, Ishiguro T. Effect of combined addition of W, Nb and V with B on the creep strengthening in high Cr ferritic heat resistant steel. Tetsu-To-Hagane 2003;89(Issue3):349–56. https://doi.org/10.2355/tetsutohagane1955.89.3_349.
[13] Nakasato F, Takahashi M. Effects of boron, titanium, and nitrogen on the hardenability of boron-treated steels for heavy machinery. Technol 1979;6(Issue1):102–5. https://doi.org/10.1179/030716979803276679.
[14] Lin H, Cheng G. Analysis of hardenability effect of boron. Mater Sci Technol 1990;6(Issue8):724–30. https://doi.org/10.1179/mst.1990.6.8.724.
[15] Melloy GF, Summon PR, Podgursky PP. Optimizing the boron effect. Metall Trans A 1973;4(Issue10):2279–89. https://doi.org/10.1007/BF02669367.
[16] Llewellyn DT, Cook WT. Metallurgy of boron-treated low-alloy steels. Technol 1974;1(Issue1):517–29. https://doi.org/10.1179/030716974803287924.
[17] Kim DS, Lee GJ, Lee MB, Hur JI, Lee JW. Manufacturing of 9CrMoCoB steel of large ingot with homogeneity by ESR process. in International Symposium on Liquid Metal Processing & Casting 2015 (LMPC2015); September 20-24; Leoben, Austria. (IOP Conference Series: Materials Science and Engineering; Vol. vol. 143). p. 12002. https://doi.org/10.1088/1757-899x/143/1/012002.
[18] Fedko J, Krucinski M. Thermodynamic analysis of boron concentration changes in steel during electroslag remelting. Ironmak Steelmak 1989;16(Issue2):116–22.
[19] Knapp WJ, Flood H. Activities in borosilicate melts: I, some melts in the system CaO–B_2O_3. J Am Ceram Soc 1957;40(Issue7):246–9. https://doi.org/10.1111/j.1151-2916.1957.tb12612.x.
[20] Dai CH, Zhang XP. A method for measuring activities in slag containing volatile component B_2O_3. Acta Metall Sin 1994;30(Issue6):243–6.
[21] Sunkar AS, Morita K. Thermodynamic properties of the MgO-$BO_{1.5}$, CaO-$BO_{1.5}$, SiO_2-$BO_{1.5}$, MgO-$BO_{1.5}$-SiO_2 and CaO-$BO_{1.5}$-SiO_2 slag systems at 1873 K. ISIJ Int 2009;49(Issue11):1649–55. https://doi.org/10.2355/isijinternational.49.1649.
[22] Huang Z, Yang Z, Su Y, Tong S, Wang Z. Activity of B_2O_3 in {(1–x) MgO +xB_2O_3} determined by (slag + metal) equilibrium at the temperature 1723 K, using copper as metal solvent. J Chem Thermodyn 1995;27(Issue12):1429–32. https://doi.org/10.1006/jcht.1995.0150.
[23] Dai C, Zhang X, Shui L. A new method for measuring activities in slags containing a volatile component. Metall Mater Trans B 1995;26(Issue3):651–4. https://doi.org/10.1007/BF02653887.
[24] Huang X, Fujisawa T, Yamauchi C. Thermodynamic properties of the MgO-$BO_{1.5}$ binary system at 1723 K. ISIJ Int 1996;36(Issue2):133–7. https://doi.org/10.2355/isijinternational.36.133.
[25] Boike M, Hilpert K, Müller F. Thermodynamic activities in B_2O_3-SiO_2 melts at 1475 K. J Am Ceram Soc 1993;76(Issue11):2809–12. https://doi.org/10.1111/j.1151-2916.1993.tb04020.x.
[26] Wang Z, Su Y, Tong S. Activity of SiO_2 in {(1–x) B_2O_3+xSiO_2} determined by (slag + metal) equilibrium at the temperature 1723 K, using (0.25 Cu + 0.75 Sn) as metal solvent. J Chem Thermodyn 1996;28(Issue10):1109–13. https://doi.org/10.1006/jcht.1996.0096.
[27] Nagai T, Ogasawara Y, Maeda M. Thermodynamic measurement of (Al_2O_3+B_2O_3) system by double Knudsen cell mass spectrometry. J Chem Thermodyn 2009;41(Issue11):1292–6. https://doi.org/10.1016/j.jct.2009.06.002.
[28] Decterov SA, Swamy V, Jung I-H. Thermodynamic modeling of the B_2O_3–SiO_2 and B_2O_3–Al_2O_3 systems. Int J Mater Res 2007;98(Issue10):987–94. https://doi.org/doi:10.3139/146.101555.
[29] Stolyarova VL, Shilov AL, Ivanov GG, Shultz MM, Seetharaman S. High temperature mass spectrometric study of the B_2O_3-Al_2O_3 system at 1248–1850 K. Rapid Commun Mass Spectrom 1995;9(Issue13):1244–51. https://doi.org/10.1002/rcm.1290091306.
[30] Stolyarova VL, Lopatin SI, Shugurov SM, Shilov AL. Thermodynamic properties of silicate glasses and melts: VII. System MgO-B_2O_3-SiO_2. Russ J Gen Chem 2010;80(Issue12):2405–13. https://doi.org/10.1134/S1070363210120029.
[31] Huang X, Asano K, Fujisawa T, Sui Z, Yamauchi C. Thermodynamic properties of the MgO-$BO_{1.5}$-SiO_2 system at 1723 K. ISIJ Int 1996;36(Issue11):1360–5. https://doi.org/10.2355/isijinternational.36.1360.
[32] Sakamoto M, Yanaba Y, Yamamura H, Morita K. Relationship between structure and thermodynamic properties in the CaO–SiO_2–$BO_{1.5}$ slag system. ISIJ Int 2013;53(Issue7):1143–51. https://doi.org/10.2355/isijinternational.53.1143.
[33] Teixeira LAV, Tokuda Y, Yoko T, Morita K. Behavior and state of boron in CaO-SiO2 slags during refining of solar grade silicon. ISIJ Int 2009;49(Issue6):777–82. https://doi.org/10.2355/isijinternational.49.777.
[34] Noguchi R, Suzuki K, Tsukihashi F, Sano N. Thermodynamics of boron in a silicon melt. Metall Mater Trans B 1994;25(Issue6):903–7. https://doi.org/10.1007/BF02662772.
[35] Jakobsson LK, Tangstad M. Thermodynamics of boron removal from silicon using CaO-MgO-Al_2O_3-SiO_2 slags. Metall Mater Trans B 2018;49(Issue4):1699–708. https://doi.org/10.1007/s11663-018-1250-7.
[36] Stolyarova VL. Mass spectrometric thermodynamic studies of oxide systems and materials. Russ Chem Rev 2016;85(Issue1):60–80. https://doi.org/10.1070/rcr4549.
[37] Peng L, Jiang Z, Geng X. Design of ESR slag for remelting 9CrMoCoB steel through experiments and thermodynamic calculations. Calphad 2020;70:101782. https://doi.org/10.1016/j.calphad.2020.101782.
[38] Pateisky G, Biele H, Fleischer HJ. The reactions of titanium and silicon with Al_2O_3-CaO-CaF_2 slags in the ESR process. J Vac Sci Technol 1972;9(Issue6):1318–21. https://doi.org/10.1116/1.1317029.
[39] Chen CX, Gao RF, Zhao WX. Effect of slag composition on Mg, Al or Ti content in Ni-based superalloy during ESR. Acta Metall Sin 1984;20(Issue3):243–51.
[40] Li S, Cheng G, Miao Z, Chen L, Li C, Jiang X. Kinetic analysis of aluminum and oxygen variation of G20CrNi2Mo bearing steel during industrial electroslag remelting process. ISIJ Int 2017;57(Issue12):2148–56. https://doi.org/10.2355/isijinternational.ISIJINT-2017-227.
[41] Yang JG, Park JH. Distribution behavior of aluminum and titanium between nickel-based alloys and molten slags in the electro slag remelting (ESR) process. Metall Mater Trans B 2017;48(Issue4):2147–56. https://doi.org/10.1007/s11663-017-0994-9.

[42] Duan SC, Shi X, Wang F, Zhang MC, Sun Y, Guo HJ, et al. A review of methodology development for controlling loss of alloying elements during the electroslag remelting process. Metall Mater Trans B 2019;50(Issue6):3055–71. https://doi.org/10.1007/s11663-019-01665-2.
[43] Zhang J, Wang P. The widespread applicability of the mass action law to metallurgical melts and organic solutions. Calphad 2001;25(Issue3):343–54. https://doi.org/10.1016/S0364-5916(01)00054-2.
[44] Jiang Z, Hou D, Dong Y-W, Cao Y-L, Cao H-B, Gong W. Effect of slag on titanium, silicon, and aluminum contents in superalloy during electroslag remelting. Metall Mater Trans B 2016;47(Issue2):1465–74. https://doi.org/10.1007/s11663-015-0530-8.
[45] Zhang J. Computational thermodynamics of metallurgical melts and solutions. Beijing: Metallurgical Industry Press; 2007.
[46] Yang X, Shi C, Zhang M, Zhang J. A thermodynamic model for prediction of iron oxide activity in some FeO-containing slag systems. Steel Res Int 2012;83(Issue3):244–58. https://doi.org/10.1002/srin.201100233.
[47] Liu Y, Zhang Z, Li G, Wu Y, Xu D, Li B. Investigation of fluoride vaporization from CaF_2-CaO-Al_2O_3 slag for vacuum electroslag remelting. Vacuum 2018;158:6–13. https://doi.org/10.1016/j.vacuum.2018.09.027.
[48] Li S, Cheng Gg, Yang L, Chen L, Yan Q, Li C. A thermodynamic model to design the equilibrium slag compositions during electroslag remelting process: description and verification. ISIJ Int 2017;57(Issue4):713–22. https://doi.org/10.2355/isijinternational.ISIJINT-2016-655.
[49] Hou D, Jiang Z, Dong Y, Cao Y, Cao H, Gong W. Thermodynamic design of electroslag remelting slag for high titanium and low aluminium stainless steel based on IMCT. Ironmak Steelmak 2016;43(Issue7):517–25. https://doi.org/10.1080/03019233.2015.1110920.
[50] Turkdogan ET. Physical chemistry of high temperature technology. New York: Academic Press; 1980.
[51] Rein RH, Chipman J. Activities in the liquid solution SiO_2-CaO-MgO-Al_2O_3 at 1600 C. Trans Metall Soc AIME 1965;233(Issue2):415–25.
[52] Xu JF, Li JC, Weng WP, Sheng MQ, Chen D, Zhang JY, et al. Calculation of surface tension for MgO-B_2O_3-SiO_2-CaO-Al_2O_3 molten boron-rich slag system. Chin J Nonferrous Metals 2017;27(Issue1):206–14.
[53] Li JX, Zhang J. Calculating model on the viscosity of CaO-MgO-MnO-FeO-CaF_2-Al_2O_3-SiO_2 slag. J Univ Sci Technol Beijing 2000;22(Issue5):438–41. https://doi.org/10.13374/j.issn1001-053x.2000.05.012.
[54] Barin I, Knacke O, Kubaschewski O. Thermochemical properties of inorganic substances: Supplement. Berlin, Heidelberg: Springer Berlin Heidelberg; 1977.
[55] Wagner C. Thermodynamics of alloys. London: Addison-Wesley Press; 1952.
[56] Fraser ME, Mitchell A. Mass transfer in the electroslag process. Part1: mass-transfer model. Ironmak Steelmak 1976;3(Issue5):279–87.
[57] Mitchell A, Joshi S. The thermal characteristics of the electroslag process. Metall Trans A 1973;4(Issue3):631–42. https://doi.org/10.1007/BF02643068.
[58] Kawakami M, Nagata K, Yamamura M, Sakata N, Miyashita Y, Goto K. Profiles of temperature, voltage and local heat generation in slag phase and metal pool of ESR unit under operation. Tetsu-To-Hagane 1977;63(Issue13):2162–71. https://doi.org/10.2355/tetsutohagane1955.63.13_2162.
[59] Narita K. Progress in electroslag remelting process. Tetsu-To-Hagane 1977;63(Issue13):1996–2009. https://doi.org/10.2355/tetsutohagane1955.63.13_1996.
[60] Hou D, Jiang Z-H, Dong Y-W, Li Y, Gong W, Liu F-B. Mass transfer model of desulfurization in the electroslag remelting process. Metall Mater Trans B 2017;48(Issue3):1885–97. https://doi.org/10.1007/s11663-017-0921-0.
[61] Hino M, Ito K. Thermodynamic data for steelmaking. Sendai: the 19th committee in steelmaking. The Japan Society for Promotion of Science, Tohoku University Press; 2010.
[62] Mitchell A, Burel B. The solution rate of alumina in CaF_2-Al_2O_3 slags. Metall Trans A 1970;1(Issue8):2253–6. https://doi.org/10.1007/BF02643442.
[63] Taira S, Nakashima K, Mori K. Kinetic behavior of dissolution of sintered alumina into CaO-SiO_2-Al_2O_3 slags. ISIJ Int 1993;33(Issue1):116–23. https://doi.org/10.2355/isijinternational.33.116.
[64] Cho WD, Fan P. Diffusional dissolution of alumina in various steelmaking slags. ISIJ Int 2004;44(Issue2):229–34. https://doi.org/10.2355/isijinternational.44.229.
[65] Bui A, Ha H, Chung I, Lee H. Dissolution kinetics of alumina into mold fluxes for continuous steel casting. ISIJ Int 2005;45(Issue12):1856–63. https://doi.org/10.2355/isijinternational.45.1856.
[66] Li JL, Shu QF, Liu YA, Chou KC. Dissolution rate of Al_2O_3 into molten CaO–Al_2O_3–CaF_2 flux. Ironmak Steelmak 2014;41(Issue10):732–7. https://doi.org/10.1179/1743281214Y.0000000187.
[67] Wu L, Gran J, Sichen D. The effect of calcium fluoride on slag viscosity. Metall Mater Trans B 2011;42(Issue5):928. https://doi.org/10.1007/s11663-011-9546-x.
[68] Park JH. Solidification behavior of calcium aluminosilicate melts containing magnesia and fluorspar. J Am Ceram Soc 2006;89(Issue2):608–15. https://doi.org/10.1111/j.1551-2916.2005.00706.x.
[69] Park JS, Kim DH, Park JH. Thermodynamic stability of spinel phase at the interface between alumina refractory and CaO–CaF_2–SiO_2–Al_2O_3–MgO–MnO slags. J Am Ceram Soc 2015;98(Issue6):1974–81. https://doi.org/10.1111/jace.13570.
[70] Tang HY, Wu GH, Wang Y, Li JS, Lan P, Zhang JQ. Comparative evaluation investigation of slag corrosion on Al_2O_3 and MgO-Al_2O_3 refractories via experiments and thermodynamic simulations. Ceram Int 2017;43(Issue18):16502–11. https://doi.org/10.1016/j.ceramint.2017.09.034.
[71] Bui A, Ha H, Kang Y, Chung I, Lee H. Dissolution behavior of alumina in mold fluxes for steel continuous casting. Met Mater Int 2005;11(Issue3):183–90. https://doi.org/10.1007/BF03027440.
[72] Wang W, Xue L, Zhang T, Zhou L, Chen J, Pan Z. Thermodynamic corrosion behavior of Al_2O_3, ZrO_2 and MgO refractories in contact with high basicity refining slag. Ceram Int 2019;45(Issue16):20664–73. https://doi.org/10.1016/j.ceramint.2019.07.049.